BULETINUL INSTITUTULUI POLITEHNIC DIN IAŞI
Publicat de
Universitatea Tehnică „Gheorghe Asachi” din Iaşi
Volumul 68 (72), Numărul 3, 2022
Secţia
CONSTRUCŢII DE MAŞINI
DOI:10.2478/bipcm-2022-0025

# A STUDY ON THE DYNAMICS OF AN AC INDUCTION MOTOR ROTOR BASED ON THE ANALYSIS OF FREE RESPONSE AT IMPULSE EXCITATION

BY

**NECULAI EDUARD BUMBU and MIHĂIŢĂ HORODINCĂ***

“Gheorghe Asachi” Technical University of Iaşi, Faculty of Machines Manufacturing and Industrial Management, D. Mangeron 59A, 700050, Iaşi, Romania

Received: September 26, 2022
Accepted for publication: September 29, 2022

**Abstract.** This paper focuses on a topic frequently involved in the dynamics of transient phenomena on rotary machines driven by an AC induction motor supplied by a three-phase four-wire electrical system: the free response of the dynamic system mirrored in the torsional vibrations of its rotor. This dynamic system is reducible at a single degree of freedom system, equivalent of a spring-mass-damper but as a torsional vibratory system composed of the motor rotor (having a moment of inertia) the rotating magnetic field (having a torsional stiffness) and a hypothetical damper (generating a viscous damping mainly due to the air friction). This free response is useful mostly to characterize the transmissibility related to the conversion of information from mechanical to electrical power through this dynamic system. A simple computer-assisted setup is used to describe indirectly and to analyze the free response (generated when the motor is switched-on or after star to delta commutation sequence), using the active electrical power absorbed by the motor.

*Corresponding author; *e-mail*: mihaita.horodinca@academic.tuiasi.ro
© 2022 Neculai Eduard Bumbu and Mihăiță Horodincă
This is an open access article licensed under the Creative Commons Attribution-NonCommercial-NoDerivatives 4.0 International License (CC BY-NC-ND 4.0).

**Keywords:** AC induction motor rotor, dynamics, free response, impulse excitation, active electrical power, transmissibility.

## 1. Introduction

When an electric motor (particularly an AC induction motor, ACIM) is used to drive a rotary machine, the evolution of the electrical absorbed power flow (an equivalent of the mechanical power flow delivered to machine) is useful for condition monitoring and diagnosis (if the active electrical power - AEP- is properly measured and processed). Some achievements on this topic (mainly in transient regimes) were previously discussed in several earlier published papers (Bumbu and Horodinca, 2022*a*, *b*; Horodinca, 2016*a*, *b*; Chifan *et al.*, 2019). A particular topic is addressed in this work: on the behaviour of the ACIM rotor system as a single degree of freedom torsional vibratory system. The transmissibility of this dynamic system (indirectly described by the free response analysis on the lowest mode of torsional vibration) is involved in the way the variable part of mechanical power (MP) is mirrored in the variable part of AEP (the amplitudes of the components of this power are amplified or diminished, depending by frequency). The sensing properties of the ACIM (revealed in the measured AEP) depends drastically by this transmissibility, especially when diagnosis in frequency domain is done. The topic of the motor rotors torsional vibrations is generally consistently discussed in the literature (in theoretical and experimental terms) as a single body vibratory system (Widdle *et al.*, 2006; Holopainen *et al*., 2013; Abdel-moamen *et al.*, 2019), sometimes as a multibody system, together with the driven equipment (Chen *et al*., 2016, Saigoa and Tanaka, 2006; Kiseleva *et al.*, 2014). The aim of these studies is generally related by a better understanding of the dynamics of the ACIM itself or together with the mechanically powered system.

Some particularly objectives are noteworthy. Thus the authors (Kiseleva *et al.*, 2014; Saigoa and Tanaka, 2006; Chen *et al.*, 2016) propose interesting approaches: the active damping systems for torsional vibrations, sometimes using the motor as actuator in a damping system. The authors (Abdel-moamen e*t al*., 2019) are interested in rotor dynamics in order to increase the dynamic stability during transient regimes. In (Widdle *et al*., 2006) the research was focussed on the elaboration of a compliant model for the rotor in order to obtain a better measurement prediction of high frequency torsional vibrations. In (Holopainen *et al.*, 2013) a study on the electromagnetic damping and stiffness for the rotor dynamics involved in drive-train electrical systems was performed. In the papers from literature based on experimental validation of the theoretical achievements, the torsional vibrations are generally revealed by torque or/and angular speed sensors (placed on rotor). In our study a simpler approach is

proposed: the evolution of the AEP absorbed by ACIM during some transient regimes. Except some particular cases which use (rarely) torsional exciters (Sihler, 2006) the torsional vibrations are generally mechanically generated (or excited) by transient regimes (this being also our approach) or electrically generated in the ACIM electrical supplying system (Holopainen *et al.*, 2013) or by a working process (Kiseleva *et al.*, 2014).

A particular approach and some achievements on the torsional free response analysis of an ACIM rotor (mirrored the AEP evolution) is exposed in this work, especially in order to find out the transmissibility of the motor used as mechanical power sensor through AEP evolution. The rest of this paper is organised as follows: Section 2 presents the experimental setup and measurement features, Section 3 focuses on AEP description, Section 4 describes the experiments, Section 5 presents the AEP signal processing results and discussion related by free responses analysis, Section 6 presents an approach on transmissibility description, Section 7 is dedicated for conclusions and future work.

## 2. The experimental setup

A conceptual description of the experimental setup (with some photos of setup components) already used and described before in (Bumbu and Horodinca, 2022*a*, *b*) is shown in Fig. 1.

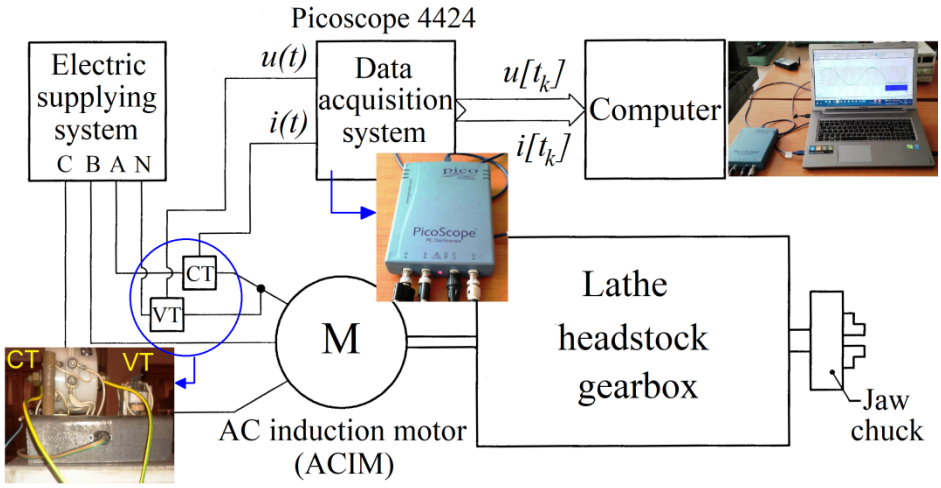



Fig. 1 – A description of the experimental setup.

Here the ACIM (1500 rpm, 5.5 KW) is directly supplied with a three-phase four-wire electrically supplying system (ESS). The ACIM starts rotation motion with a star-delta starting procedure, this being also the way to excite and

to produce a free torsional response of the dynamic system of the rotor. The ACIM rotor drives mechanically a lathe headstock gearbox (partially involved in this study). On the phase A from ESS, a current transformer CT is placed. It provides the instantaneous current $i(t)$ in analog format, delivered to an oscilloscope PicoScope 4424 (four channel, 12 bits numerical resolution, from Pico Technology UK) as data acquisition system. Between the phase A and the neutral wire N of ESS a voltage transformer VT is placed. It provides the instantaneous voltage $u(t)$ in analog format to the same data acquisition system. The oscilloscope converts the analog inputs $i(t)$ and $u(t)$ in numerical outputs having samples generically written as $i[t_k]$ and $u[t_k]$. An appropriate sampling rate is used (100,000 $s^{-1}$) with $\Delta t$=1/100,000 s=10 μs as sampling time. These samples are delivered to a computer for numerical processing (mainly AEP signal synthesis and free response analysis). The numerical samples $P[t_l]$ of the absorbed AEP by ACIM depends strictly only by $i[t_k]$ and $u[t_k]$ samples. The instantaneous current (IC) and instantaneous voltage (IV) have with a good approximation sinusoidal evolution, with period a $T$ (20 ms for 50 Hz AC frequency).

## 3. Some considerations on numerical AEP definition

First simple available definition useful in AEP definition is the instantaneous electrical power (IEP), with a generic sample $p[t_k]$ defined as:

$$p[t_k] = 3 \cdot u[t_k] \cdot i[t_k] \tag{1}$$

A multiplication factor 3 is used because the ACIM is supplied by three phases since the IV and IC are measured on a single phase. For a better description of transient phenomena IEP is replaced by AEP, with a definition of a single sample $P$ (already depicted in Bumbu and Horodinca, 2022*a*) as the average of IEP on a semi-period $T/2$:

$$P = \frac{3}{n \cdot \Delta t} \sum_{k=1}^{k=n} u[t_k] \cdot i[t_k] \cdot \Delta t = \frac{3}{n} \sum_{k=1}^{k=n} u[t_k] \cdot i[t_k] \tag{2}$$

Here $n$ is the number of samples $i[t_k]$ and $u[t_k]$ on a semi-period (ideally $T/2=n \cdot \Delta t$). Usually $n$ accomplishes the best this relationship as the integer of the ratio $T/(2 \cdot \Delta t)$. This definition assures two samples of AEP on each period $T$, or 100 samples on each second (or a sampling rate of 100 $s^{-1}$). This definition basically eliminates the main variable component inside IEP with 100 Hz frequency (sinusoidal in stationary regimes), electrically generated.

A better approach of AEP definition is available using a moving average filter ($n$ samples in the average) with a jump over $s$ samples ($s < n$). A sample of AEP is generically described as a:

$$P_1[t_l] = \frac{3}{n} \cdot \sum_{k=s\cdot(l-1)+1}^{s\cdot(l-1)+n} p[t_k] \tag{3}$$

If there are available $m$ IV and $m$ IC samples ($k_{max}=m$) then mandatory this relationship $s\cdot(l\text{-}1)+n \leqslant m$ should be attained. The sample time $t_l$ of the $l^{th}$ sample $P_1$ from Eq. (3) is defined as:

$$t_l = \frac{2 \cdot s \cdot (l-1) + n}{2} \cdot \Delta t \tag{4}$$

The definition from Eq. (3) keeps the advantage of definition from Eq. (2) related by removing the dominant component (100 Hz frequency) from IEP, but supplementary removes the harmonics of this component (100, 200… Hz). In addition the definition (3) increases a lot the sampling rate which now is selectable: there are $n/s$ samples on each semi-period $T/2$. If $s=1$ then $t_l = t_k$, in other words AEP has the same number of samples and the same sampling rate with IEP. If $s=n$ then the definition from Eq. (3) becomes the definition from Eq. (2) particularly written for $l=1$.

All the calculus, signal processing procedures and graphical representation of signals evolutions were done using appropriate programs written in Matlab.

## 4. The description of the experiments by IAP and AEP evolutions

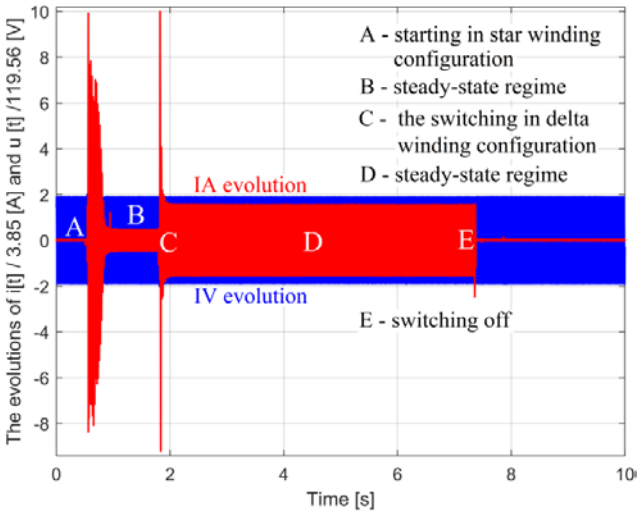



Fig. 2 – The evolution of IV and IC during a sequence of start-stop procedure of ACIM.

The easiest way to excite the free response is the star-delta starting procedure. Figure 2 presents simultaneously the evolution of a signal proportional with IV (delivered by VT) and IC (delivered by CT) during a short sequence of starting and stopping procedure of ACIM (without any mechanical loading at rotor, ACIM being completely separated by lathe headstock gearbox). Because VT is placed before the electrical switcher the events between start (A) and stop (E) moments is described only by the evolution of IC (since IV is apparently constant). However IV is slightly variable, according with the results from a previous work (Bumbu and Horodinca, 2022*a*). As expected, there is a strong variation of the IC amplitude during transient regimes (revealed in A and C, because of mechanical dynamics due to a strong acceleration) and relatively constant IC amplitude during steady-state regimes (in B and D). The evolution of IC is an important indicator useful to describe the ACIM behavior during transient regimes. Figure 3 depicts a zoom-in detail of Fig. 2 in area C. Here will be localized the free response of the dynamic system of the ACIM rotor, revealed later in the evolution of AEP.

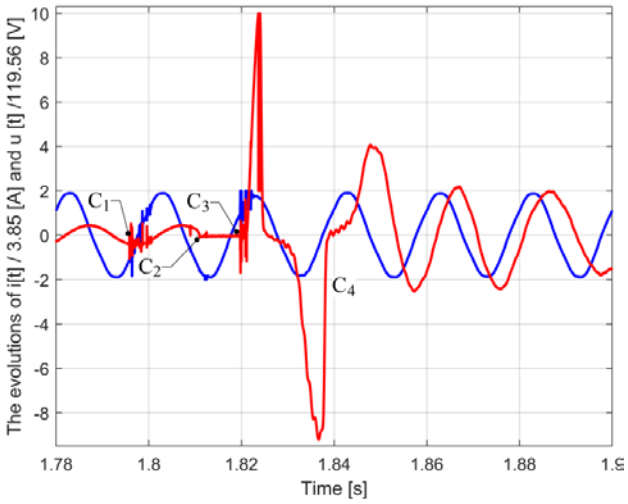



Fig. 3 – A zoom-in detail in the area C of Fig. 2.

In $C_1$ start the commutation phenomena from star to delta configuration. In $C_2$ the ACIM is for a short time completely disconnected from electrical supplying network (between $C_2$ and $C_3$ IC is zero). In $C_3$ the ACIM stator (which generates the rotating magnetic field) is electrically connected in delta winding configuration. In this moment really starts the transient regime C from Fig. 2. This transient regime (due to the acceleration of the rotor) is characterized by a strong deformed regime of IC (*e.g.* in $C_4$ moment). The shift of phase between IV and IC is clearly indicated (before $C_1$ and after $C_4$). While the IV frequency is constant, during this deformed regime (which occurs

similarly also in area A on Fig. 2) the definition from Eq. (3) for AEP remains fully available.

Figure 4 describes the evolution of IEP and AEP during the start-stop sequence described in Fig. 2. The IEP samples were calculated with Eq. (1). The AEP samples were calculated using Eq. (3) with $n$=1000 and $s$=1.

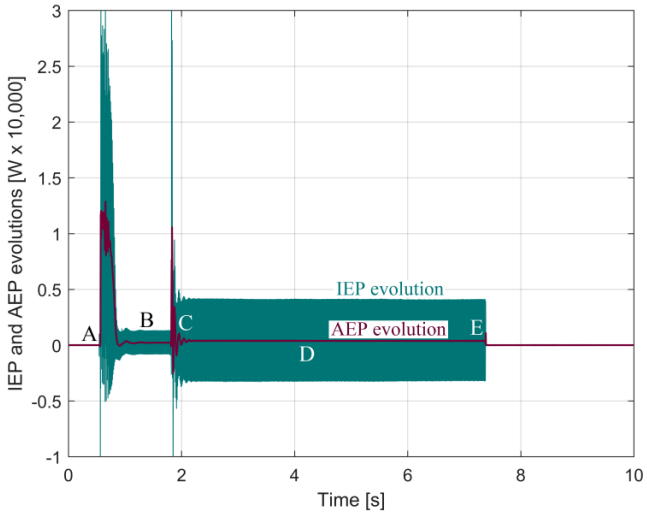



Fig. 4 – The IEP and AEP evolutions during the sequence depicted in Fig. 2.

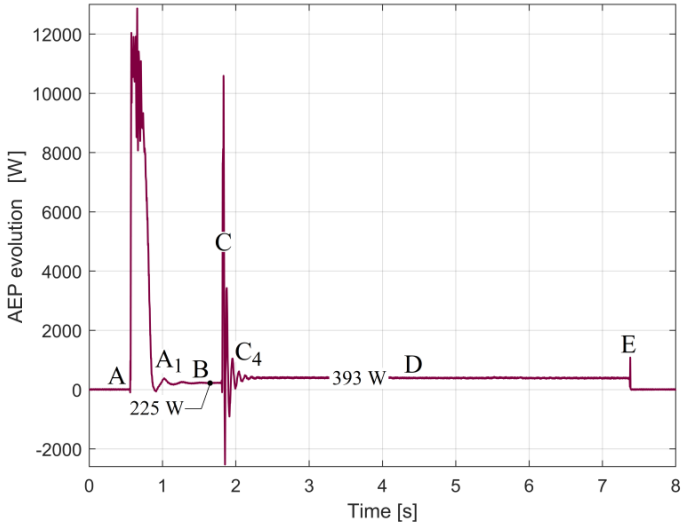



Fig. 5 – The AEP (partially) evolution during the sequence depicted in Fig. 2 (also revealed in Fig. 4).

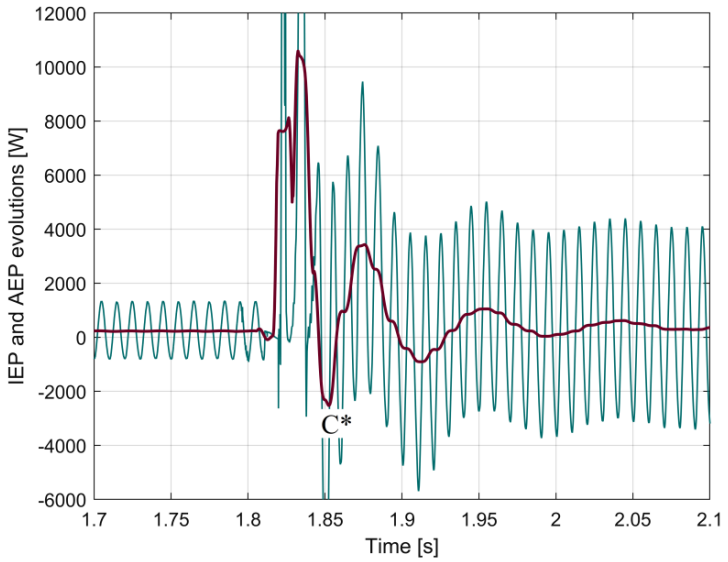



Fig. 6 – A zoom-in detail on Fig. 5 in C and $C_4$ areas (with IEP and AEP evolutions).

Figure 5 presents only the evolution of AEP. Some interesting issues are available here, first being the evolution of AEP during transient regimes with a free response of the ACIM rotor dynamic system in $A_1$ (after the connection in star configuration) and $C_4$ (after the connection in delta configuration). This last response from $C_4$ (detailed in Fig. 6) will be analyzed later in order to detect the dynamic properties (natural angular frequency and damping degree) useful to describe theoretically the evolution of the transmissibility. We should mention that in A and C there are two significant peaks of AEP (bigger than 10 KW). This is the main reason for a star-delta configuration of winding used for ACIM rotation starting (if the motor starts directly in delta configuration the peak of AEP is too big, this being dangerous for ACIM and ESS). The AEP absorbed when ACIM runs in steady-regime (in D) is roughly 393 W.

## 5. The analysis of the rotor dynamic system free responses by curve fitting

It is obviously that, starting with the moment C* (on Fig. 6, as an origin of time), the AEP evolution describes a free damped response after an impulse excitation. This response describes the free torsional vibrations of the ACIM rotor. It has a presumed well known theoretical model as it follows:

$$P_{fr}(t) = P_{ss} + a \cdot e^{-\zeta \cdot \omega_n \cdot t} \sin(\omega_d \cdot t + \varphi) \quad (5)$$

Here $P_{ss}$ is a constant power (steady-state AEM in D on Fig. 5, with $P_{ss}$ = 393 W), $a$ is an initial amplitude, $e$ is the Euler's number, $\zeta$ is the viscous damping factor, $\omega_n$ is the angular natural frequency of the system (if the damping in system is neglected), $\omega_d$ is the angular damped frequency of the system (if the damping is not neglected), $\varphi$ is the phase shift at origin of time (the moment C*, when $t$=0). First challenge is to confirm that Eq. (5) is really a theoretical description of the experimental free response. Second challenge is to find the values of the constants $a$, $\zeta$, $\omega_n$, $\omega_d$ and $\varphi$ which ensures that a theoretical evolution described by Eq. (5) having these constants implies the best possible fit with the experimental evolution. Both challenges are solvable by so called curve fitting procedure. A common way to solve this issue is to use the Curve fitting Toolbox™ software from Matlab (CFTM). In our work an appropriate algorithm and computer program for curve fitting (also in Matlab) were developed as a theoretical approach (as OCFP, from our curve fitting procedure) already fully confirmed in a previous work on free damped response analysis (Horodinca, 2016a, b).

However the OCFP has a relative severe disadvantage: it runs slowly by comparison with CFTM, but it has also an interesting advantage: it allows applying an original approach. Firstly the value $P_{ss}$ was subtracted from experimental evolution (in Eq. (5) only the second term is used for curve fitting). Secondly for each constant, a range $a_{min} \div a_{max}$, $\zeta_{min} \div \zeta_{max}$, $\omega_{n\,min} \div \omega_{n\,max}$, $\omega_{d\,min} \div \omega_{d\,max}$ and $\varphi_{min} \div \varphi_{max}$ is established, basically by approximation or using some skills in this study (e. g the difference $\varphi_{max} - \varphi_{min}$ should not exceeds $2\pi$). Each constant have successively $a_i$, $\zeta_i$, $\omega_{ni}$, $\omega_{di}$ and $\varphi_i$ values inside its range during fitting procedure. Let be two AEP generic numerical samples: a sample $P_{fre}[t_l]$ on experimental free response and a sample $P_{frt}^{i}[t_l]$ on theoretical free response (calculated with Eq. (5) and the constants $a_i$, $\zeta_i$, $\omega_{ni}$, $\omega_{di}$ and $\varphi_i$). Suppose that there are $h$ AEP experimental samples. The fitting procedure means to find out that value $i=i_{ba}$ (which defines the best appropriate values constants $a_{iba}$, $\zeta_{iba}$, $\omega_{niba}$, $\omega_{diba}$ and $\varphi_{iba}$) which ensures the fulfillment of this relationship:

$$\varepsilon = \sum_{l=1}^{h} \left| P_{fre}[t_l] - P_{frt}^{iba}[t_l] \right| \rightarrow min \tag{6}$$

In ideal condition (if the theoretical model describe perfectly the experimental evolution and if the values of the constants are perfectly determined) $\varepsilon$ should be zero.

During the fitting procedure it is obviously that it is impossible to find out the correct values for $\zeta$ and $\omega_n$ separately but is possible to find the right value of the result of multiplication $\zeta \cdot \omega_n$. In order to have an approximate description of viscous damping factor $\zeta$ it is possible to consider that $\omega_n = \omega_d$

(with $\zeta$ having small value, there is a small difference between $\omega_n$ and $\omega_d$, with $\omega_d = \omega_n\sqrt{1-\zeta^2}$ as established by vibration literature) and to rewrite Eq. (5) in a simpler manner, as:

$$P_{fr}(t) \approx P_{ss} + a \cdot e^{-\zeta \cdot \omega_d \cdot t} \sin(\omega_d \cdot t + \varphi) \tag{7}$$

Now there are only four different constants involved in curve fitting procedure ($a$, $\zeta$, $\omega_d$ and $\varphi$) and the curve fitting procedure becomes simpler.

Figure 7 depicts the result of OCFP for the fitting of free response from Fig. 6, starting with the moment C* (on Fig. 6). Despite a noisy evolution of the experimental free response, it is obvious that it fits quite well with the theoretical response (depicted in magenta color). In order to reduce the time of curve fitting procedure in the description of AEP (from Eq. (3)) here $s$=100, and $h$=330. There are $n/s$=1000/10=10 AEP samples on each semi period $T/2$. In order to increase the curve fit precision, the program can be run few times, every time the range of each constant being severely diminished around the value previously found.

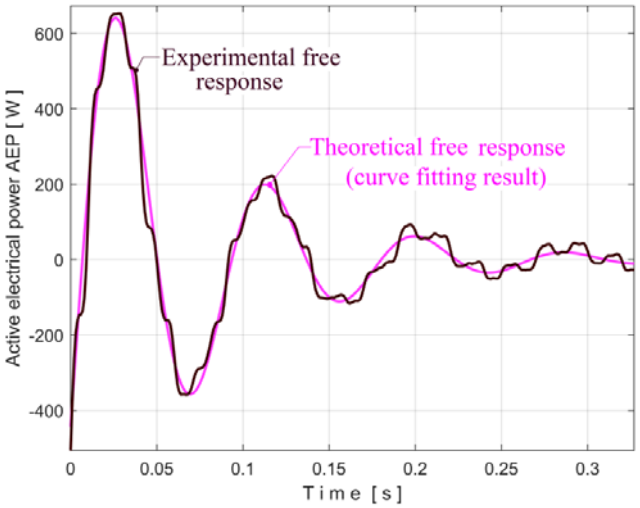



Fig. 7 – The graphical result of curve fitting (by OCFP method) on AEP of ACIM rotor dynamic system free response.

In first two rows of Table 1 are described by comparison the values of constants determined by both curve fitting procedures (CFTM and OCFP). The last column describes the sum of squares due to error (SSDE, a description of fitting quality), calculated as:

$$SSDE = \sum_{l=1}^{h} \left(P_{fre}[t_l] - P_{frt}^{ia}[t_l]\right)^2 \tag{8}$$

Despite the huge running time of OCFP, the both curve fitting methods produces quite similar results and the same SSDE (even insignificantly smaller for OCFP). The previously considered relationship $\omega_d = \omega_n\sqrt{1-\zeta^2}$ produces (with $\zeta$, $\omega_d$ OCFP results) the value $\omega_n$=73.281 rad/s while $\omega_d$ = 72.03 rad/s.

The experimental AEP free response from Fig. 7 contains a supplementary variable component. This is an electrically generated 50 Hz sinusoidal component with period *T*. It is possible to completely remove this component if a moving average filter with 2*n*/*s*=20 samples in the average (samples per period *T*) is applied (as a low-pass filter) before fitting.

**Table 1**

*The values of constants (a, ζ, $\omega_d$ and φ) from Eq. (7) deduced by curve fitting of the experimental free response (with the ACIM rotor free of any loading)*

| Fitting procedure | *a* [W] | $\zeta$ [ rad$^{-1}$] | $\omega_d$ [rad/s] | $\varphi$ [rad] | Running time [s] | SSDE [W$^2$] |
|---|---|---|---|---|---|---|
| CFTM | 909.3 | *0.1824* | *72.79* | 5.765 | negligible | 303,300 |
| OCFP | 920.3 | *0.1840* | *72.03* | 5.809 | 83 | 329,600 |
| OCFPF | 890.33 | *0.1818* | *72.66* | 5.497 | 84 | 80,832 |
| | | $\bar{\zeta}$***=0.1827*** | $\bar{\omega}_d$*=72.48* | $\bar{\omega}_n$*=73.72* rad/s | | |

On this filtered AEP free response the curve fitting procedures can be also applied (*e.g.* using OCFP renamed now OCFPF). Similarly with Fig. 7, Fig. 8 presents the graphical result of OCFPF.

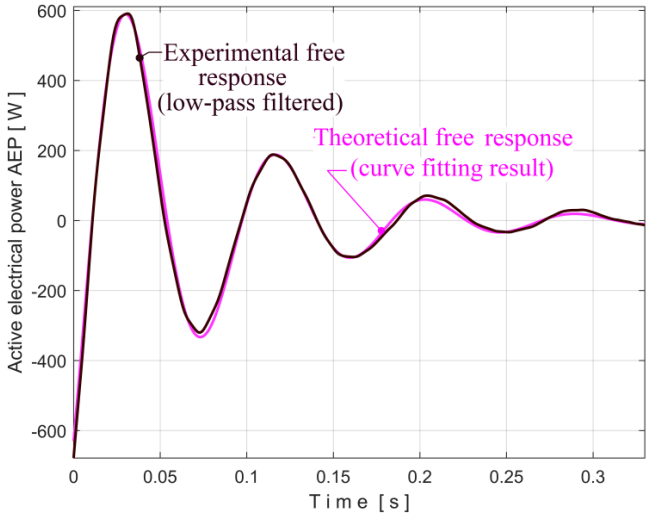



Fig. 8 – The graphical result of curve fitting (by OCFPF) on filtered AEP of ACIM rotor dynamic system free response.

In the third row of Table 1 the constants determined by OCFPF procedure are described. It is evident that the amplitude $a$ and the phase shift $\varphi$ are strongly changed and SSDE strongly shrinks because of filtering but, as expected, the viscous damping factor $\zeta$ and the angular natural frequency $\omega_d$ keep relatively the same values with CFTM and OCFP fitting methods. Because these two constants are useful to describe the ACIM rotor dynamic system transmissibility, the best approach is to consider the average values (on three fitting procedures from Table 1) as $\bar{\zeta}$= 0.1827 rad$^{-1}$ and $\bar{\omega}_d$=72.48 rad/s, which define the average value $\bar{\omega}_n$=73.72 rad/s.

By curve fitting two issues were achieved: a good validation of the (adapted) theoretical model of free response from Eq. (7) and the finding of the appropriate values of the four constants involved in theoretical description of an experimental free response (on AEP) using this model. For some reasons, mainly due to an imperfect model, (Horodinca, 2016*a*, *b*), the theoretical and experimental evolutions from Fig. 8 don't perfectly fit. It is obvious that the main free response constants ($\zeta$ and $\omega_d$) strongly depend by ACIM rotor dynamics. As example, in area $A_1$ on Fig. 5 there is also a free response immediately after ACIM starts in star winding configuration. The $\omega_d$ value is strongly smaller now because a smaller current implies smaller rotating magnetic field stiffness. A mechanical loading applied on ACIM rotor implies also the changing of damping and frequency of the free response, according with the results of a new experiment.

Now the ACIM rotor drives only a flat belt transmission FBT and a driven shaft DS (Fig. 9) placed at the input of the lathe headstock gearbox (Bumbu and Horodinca, 2022*a*, *b*).




Fig. 9 – The flat belt transmission.

Figure 10 presents the AEP evolution ($n$=2000, $s$=1) during a sequence of star-delta starting procedure of ACIM. By comparison with Fig. 5 the steps from A to D are similarly highlighted. Due to dry and wet friction introduced by FBT and DS the AEP consumption in B and D steady-state situations is significantly. The free response in $A_1$ is missing but still exists in $C_4$. An analysis of this new free response (243 AEP samples, $n$=2000, $s$=200, and 20 samples on each period $T$) was done by CFTM, OCFP and OCFPF procedures (with the determined constants depicted in Table 2).

**Table 2**

*The values of constants ($a$, $\zeta$, $\omega_d$ and $\varphi$) from Eq. (7) deduced by curve fitting of a new experimental free response (with FBT and DS driven by the ACIM rotor)*

| Fitting procedure | $a$ [W] | $\zeta$ [ rad$^{-1}$] | $\omega_d$ [ rad/s] | $\varphi$ [rad] | Time [s] | SSDE [W$^2$] |
|---|---|---|---|---|---|---|
| CFTM | 3143 | *0.3441* | *66.65* | 5.743 | negligible | 4,599,000 |
| OCFP | 2901 | *0.3149* | *68.89* | 5.65 | 63 | 5,298,269 |
| OCFPF | 2870 | *0.3106* | *69.10* | 5.77 | 70 | 2,186,563 |
| | | ***$\bar{\zeta}$=0.3232*** | *$\bar{\omega}_d$=68.213* | *$\bar{\omega}_n$=72.081 rad/s.* | | |

Figure 11 depicts the graphical result of OCFP; Figure 12 depicts the graphical results of OCFPF on filtered evolution of AEP.

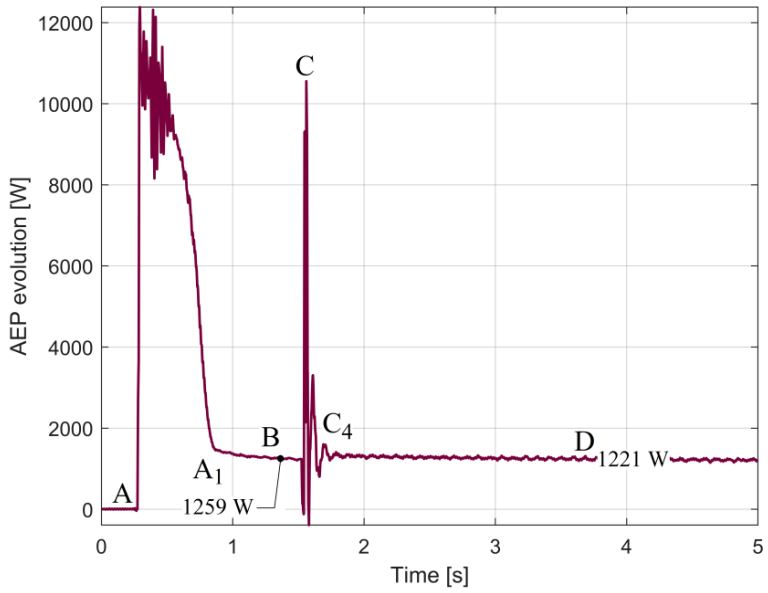



Fig. 10 – The evolution of AEP during a sequence of star-delta starting procedure of ACIM (which drives a flat belt transmission FBT).

Here in Fig. 12, in opposition with the result from Fig. 8, it is evident that the theoretical model of free response from Eq. (7) is badly adapted with the experimental evolution (the dry friction is not considered in model).

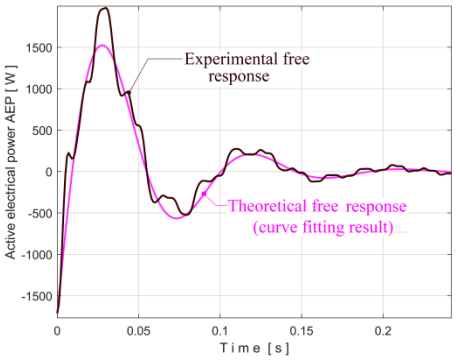



Fig. 11 – The graphical result of curve fitting (by OCFP) on AEP of ACIM rotor dynamic system free response (from $C_4$ on Fig. 10).

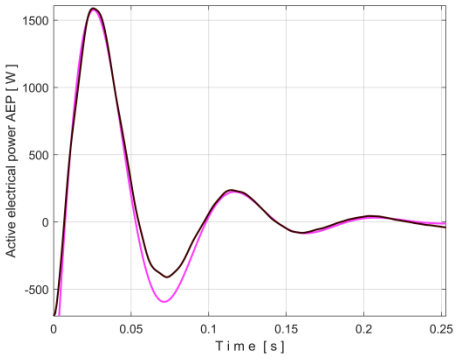



Fig. 12 – The graphical result of curve fitting (by OCFPF) on AEP of ACIM rotor dynamic system filtered free response (from $C_4$ on Fig. 10).

The values from Table 2 help to define the average constants $\bar{\zeta}$= 0.3232 rad$^{-1}$ and $\bar{\omega}_d$=68.213 rad/s which defines $\bar{\omega}_n$=72.081 rad/s. As expected, this time the damping is significantly bigger since the angular frequencies roughly keeps the same values. This angular frequency is proportional with the ratio between the stiffness of the rotating magnetic field and the total moment of inertia (the total moment of inertia increases due to DS but also increases the stiffness of rotating magnetic field due to the increasing of the absorbed current).

## 6. An approach on the transmissibility of the rotor dynamic system

When the sensing properties of ACIM are used for indirectly MP measurement (by computer assisted AEP measurement), the analytical description of free response of the ACIM rotor motor dynamic system is useful especially to describe approximately the transmissibility, involved in the description of MP variable (sinusoidal) parts in AEP. This transmissibility describes how the amplitude of a MP sinusoidal component is changed when is mirrored in AEP, or the evolution of ratio (amplitude AEP)/(amplitude MP) versus frequency. Probably the best approach on the theoretical description of this transmissibility is given by the analogy with the transmissibility $A_0$ of a single degree of freedom vibration isolator system, written as depending by excitation frequency $f$:

$$A_0(f) = \frac{\sqrt{1 + (2\bar{\zeta}\frac{2\pi f}{\bar{\omega}_n})^2}}{\sqrt{\left[1 - \left(\frac{2\pi f}{\bar{\omega}_n}\right)^2\right]^2 + (2\bar{\zeta}\frac{2\pi f}{\bar{\omega}_n})^2}} \quad (9)$$

With the average values of constants $\bar{\zeta}$ and $\bar{\omega}_n$ involved in Eq. (9) already determined as a results of previously experiments by curve fitting (described in Tables 1 and 2) it is possible to build the theoretical evolutions of the transmissibility, as Fig. 13 indicates.

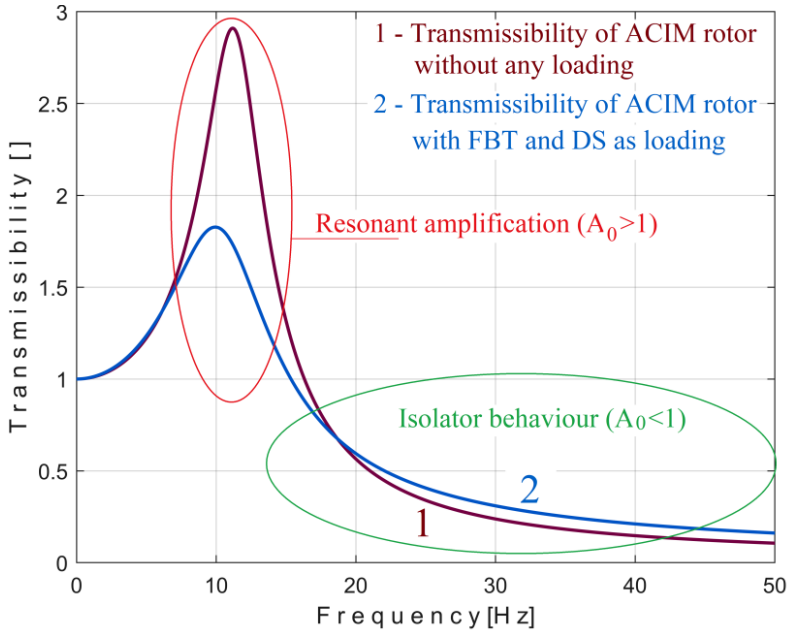



Fig. 13 – The evolution of dynamic transmissibility of the ACIM rotor dynamic system $A_0(f)$ based on Eq. (9) and experimental results ($\bar{\zeta}$ and $\bar{\omega}_n$) from Tables 1 and 2.

It is clear here that, mainly due to a small damping, the transmissibility is far from having the ideal evolution ($A_0$=1 whatever the frequency is) in both experimental situations (depicted here with 1 and 2). The amplitudes of some MP components with the frequency placed in resonant area will be amplified in AEP due to the resonance phenomenon (with a stronger amplification on curve 1, almost free times at resonance frequency), the amplitude of some other MP components with the frequency placed in isolation area will be strongly diminishes (practically similarly on both curves). Here the ACIM rotor dynamic

system works as a low pass filter for MP components. With a known theoretical evolution of the transmissibility a correction of the amplitude of each sinusoidal AEP component (having the known frequency $f$) can be simply done by multiplication with $1/A_0(f)$.

A better approach on the evolution of this transmissibility is possible if a sinusoidal MP with constant amplitude and selectable frequency is produced as loading at the ACIM rotor (a torque sensor is necessary). For each of these sinusoidal MP (having known frequency) the AEP amplitude is measured. The transmissibility results as the evolution of ratio (amplitude AEP)/(amplitude MP) versus frequency.

This topic of transmissibility evolution based on free response of ACIM rotor (when ACIM is used for sensing purposes based on AEP evolution) is suitable for simple rotary driven system. The motorized spindle used in CNC machine-tools (the ACIM rotor is also the spindle) can be fully considered as such a system. This topic was briefly addressed in a previous work (Chifan *et al*., 2019).

## 7. Conclusions and future work

This paper focuses on the dynamic behaviour of an AC induction motor as loading sensor involved in the description of variable components of mechanical power mirrored in the evolution of active electrical power. The main attainment of this work was the proposal of a theoretical and experimental approach based on a simple setup and experiment (free response of rotor dynamic system at impulse excitation in transient regimes) focused on the dynamic transmissibility description. This approach was fully accomplished based on some original achievements:

- a simple method of active electrical power monitoring was proposed, based on instantaneous current and voltage acquired at the motor electrical input.
- a simple experimental setup with numerical signal acquisition and processing facilities based on sensing properties of an AC induction motor was proposed and used in experimental research.
- a transient regime able to generate a free viscous damped response was detected and experimentally addressed.
- a computer assisted method for active electrical power analysis (curve fitting) was proposed in order to find out the best theoretical description of the free viscous damped response.
- a proposal on an indirect method of deducing the evolution of transmissibility.

A future approach will be focused on the computer assisted analysis of the free responses of motorized spindles used in CNC milling machines mirrored in the absorbed active electrical power evolution.

## REFERENCES


Abdel-moamen D., Abdel-Rhman M., Swief R.A., Abdel-Lattif Badr M., *On the Natural Frequency of Oscillations of Induction Motors*, The Academic Research Community publication, ISSN: 2537-0154, **2** (4), 398-408 (2019).

Bumbu E.N., Horodinca M., *The Mirroring of a Transient Regime of a Lathe Headstock Gearbox in the Evolution of Supplying Voltage of the AC Driving Motor*, RECENT, ISSN 1582-0246, **23** (1(66)), 21-30 (2022a).

Bumbu E.N., Horodinca M., *A Study on the Evolution of the Supplying Current Absorbed by an AC Driving Motor During a Transient Regime on a Lathe Headstock Gearbox*, Bulletin of the Polytechnic Institute of Iaşi. Machine Constructions Section, **68** (1), 25-34 (2022b).

Chen K., Hu J., Peng Z., *Analysis of torsional vibration in an electromechanical transmission system*, Advances in Mechanical Engineering, **8**(6) 1-9 (2016).

Chifan F., Luca C., Horodinca M., Dumitras C.G., *An Approach on a Transient Regime of a CNC Machining Center Spindle Drive System Using the Active Electrical Power Evolution*, RECENT, ISSN 1582-0246, **20** (3(59)), 99-106 (2019).

Holopainen T.P., Niiranen J., Jörg P., Andreo D., Electric *Motors and Drives in Torsional Vibration Analysis and Design*, Proceedings of the Forty-Second Turbomachinery Symposium, Houston, Texas, USA, October 1-3, 2013.

Horodinca M., *The Monitoring of Transient Regimes on Machine Tools Based on Speed, Acceleration and Active Electric power Absorbed by Motors*, Modtech International Conference - Modern Technologies in Industrial Engineering IV, Iasi, Romania, June 15-18, 2016a.

Horodinca M., *Experimental Investigation of Free Response on a Cantilever Beam (First Flexural Vibration Mode)*, Bulletin of the Polytechnic Institute of Iaşi. Machine Manufacturing Section, **62(66)** (3), 23-34 (2016b).

Kiseleva M.A., Kondratyeva N.V., Kuznetsov N.V., Leonov G.A., Solovyeva E.P., *Hidden periodic oscillations in drilling system driven by induction motor*, Proceedings of the 19th World Congress the International Federation of Automatic Control IFAC, Cape Town, South Africa, August 24-29, (2014).

Saigoa M., Tanaka N., *Torsional vibration suppression by wave absorption controller*, Journal of Sound and Vibration **295,** 317-330 (2006).

Sihler C., *A novel torsional exciter for modal vibration testing of large rotating machinery*, Mechanical Systems and Signal Processing **20,** 1725-1740 (2006).

Widdle Jr.R.D., Krousgrill Jr.C.M., Sudhoff S.D., *An induction motor model for high-frequency torsional vibration analysis*, Journal of Sound and Vibrations **290**, 865-881 (2006).


## UN STUDIU ASUPRA DINAMICII UNUI MOTOR DE CURENT ALTERNATIV BAZAT PE ANALIZA RĂSPUNSULUI LIBER LA EXCITAȚIA DE TIP IMPULS

(Rezumat)


Această lucrare cercetează un subiect de interes din dinamica fenomenelor tranzitorii la mașinile (sistemele mecanice) acționate de un motor de curent alternativ

alimentat cu un sistem electric trifazat: răspunsul liber al sistemului dinamic oglindit în vibrațiile de torsiune ale rotorului său. Acest sistem dinamic este reductibil la un singur grad de libertate, echivalent al unui sistem arc-masă-amortizor care se manifestă prin vibrații de torsiune, compus din rotorul motorului (având moment de inerție), câmpul magnetic rotativ (având rigiditate torsională) și un ipotetic amortizor (generând o amortizare vâscoasă, în principal datorită frecării cu aerul). Acest răspuns liber este util mai ales pentru a caracteriza transmisibilitatea legată de conversia informației din puterea mecanică în puterea electrică prin intermediul acestui sistem dinamic. Un stand experimental simplu, asistat de calculator, este utilizat pentru a descrie și pentru a analiza răspunsul liber (generat la pornirea motorului sau după o secvență de comutare stea-triunghi), folosind puterea electrică activă absorbită de motor.